Noise characterization of ultrasensitive anomalous Hall effect sensors based on $Co_{40}Fe_{40}B_{20}$ thin films with compensated in-plane and perpendicular magnetic anisotropies (EP)

(iD) Yiou Zhang, (iD) Kang Wang and (iD) Gang Xiao

COLLECTIONS

EP This paper was selected as an Editor's Pick

View Online   Export Citation   CrossMark

ARTICLES YOU MAY BE INTERESTED IN

Noise characterization of ultrasensitive anomalous Hall effect sensors based on $Co_{40}Fe_{40}B_{20}$ thin films with compensated in-plane and perpendicular magnetic anisotropies (EP)

Yiou Zhang, (ID) Kang Wang, (ID) and Gang Xiao[a] (ID)

AFFILIATIONS

Department of Physics, Brown University, Providence, Rhode Island 02912, USA

[a] Author to whom correspondence should be addressed: Gang_Xiao@Brown.edu

ABSTRACT

We have performed magnetotransport and noise characterization studies of ultrasensitive anomalous Hall effect (AHE) sensors based on the $Ta/Co_{40}Fe_{40}B_{20}/MgO$ multilayer structure. The magnetization is near spin reorientation transition. This greatly reduces the saturation field with improvement of the magnetic sensing performance. We have performed temperature-dependent measurements to investigate the effect of tunable magnetic anisotropy. Both $1/f$ noise and sensitivity have a strong temperature dependence. Moreover, the scaling relations between $1/f$ noise and sensitivity change dramatically as temperature changes, showing different noise originations depending on magnetic anisotropies. With a small sensing area of $20 \times 20\,\mu m^2$, the best magnetic field detectability reaches $76\,nT/\sqrt{Hz}$ at $1\,Hz$ and $2\,nT/\sqrt{Hz}$ at $10\,kHz$. AHE sensors with compensated magnetic anisotropies are, thus, suitable for ultrasensitive magnetic field sensing applications.

Published under license by AIP Publishing. https://doi.org/10.1063/5.0008949

The anomalous Hall effect (AHE) has attracted increasing attention in recent years, both in fundamental physics[1–3] and in magnetic field sensing applications.[4–9] AHE sensors based on magnets are relatively easy to fabricate, have lower intrinsic noise,[5] and can operate in a large frequency range.[10] Nevertheless, AHE sensors still suffer from low sensitivity, as compared to commercially available semiconductor Hall sensors. One approach to improve the sensitivity of AHE sensors is to enhance the anomalous Hall resistivity. Topological insulators[6] or Weyl semimetals[1–3,11] have non-trivial band structures, giving rise to the large AHE due to the Berry-curvature contribution. However, such an effect is only present at quite low temperatures in most materials, which hinders their applications.

Besides increasing the anomalous Hall resistivity, reducing the saturation field of magnets can also enhance the sensitivity of AHE sensors. Due to the large in-plane anisotropy of the thin film structure, the saturation field typically reaches a few Tesla,[12,13] inducing a low sensing capability. On the other hand, a perpendicular magnetic anisotropy can be promoted through interfacial electronic hybridization.[14–16] A strong perpendicular anisotropy leads to not only a small saturation field but also a large coercivity. This allows for applications in magnetic memory instead of magnetic field sensing. When magnetization is near spin reorientation transition from perpendicular magnetization to in-plane magnetization, a linear and reversible anomalous Hall loop with a small saturation field can be achieved.[8] AHE sensors with compensated in-plane and perpendicular magnetic anisotropies can have a sensitivity as high as a few thousands of Ω/T,[4,8,9,17] comparable to or even exceeding that of the semiconductor Hall sensors, which are desirable for ultrasensitive magnetic field sensing.

In addition to achieving high sensitivity, reaching low intrinsic noise is also of great significance to achieve a good sensing performance. So far, there has been little work on noise characterization of AHE sensors. Our early work on AHE sensors based on FePt alloys with in-plane anisotropy has shown that the AHE sensor has much lower low-frequency noise and, thus, outperforms semiconductor Hall sensors in the low-frequency region.[5] Shiogai *et al.*[18] also showed that the AHE sensor based on nanocrystalline FeSn has a comparable performance to semiconductor Hall sensors. Nevertheless, it remains an open question how the tunable magnetic anisotropies near spin reorientation transition affect the intrinsic noise of AHE sensors. Noise characterization of AHE sensors with tunable magnetic anisotropies is essential for understanding and optimization of AHE sensors.

In this work, we have chosen $Ta/Co_{40}Fe_{40}B_{20}/MgO$ as the basic structure of the AHE sensor, which is more cost-effective than Pt-based multilayers or alloys. Magnetic anisotropy has a strong temperature dependence.[19,20] This provides one way to fine-tune the effective magnetic anisotropy in a single magnetic sensor. We have performed comprehensive magnetotransport and noise characterization of the AHE sensor in the range of 250 K–350 K and in a broad frequency range of 1 Hz to 10 kHz. We have observed and analyzed the interplay of $1/f$ noise and sensitivity, as well as the magnetic field detectability, with tunable magnetic anisotropies.

For our studies, we deposited multilayers of $Ta(1.6)/Co_{40}Fe_{40}B_{20}(0.9)/MgO(1.6)/TaO_x(1.0)$ (layer thicknesses in nanometers) on thermally oxidized silicon wafers using a custom multitarget high-vacuum magnetron sputtering system. The multilayer stacks were patterned into a Hall bar structure, as shown in Fig. 1(a), through standard photolithography and ion-milling processes. The active sensing area of a Hall bar is $20 \times 20 \ \mu m^2$. The sheet resistance is $3 \ k\Omega/sq$. Cr/Au layers were deposited and lift off to form contact electrodes to current and voltage leads. Post-growth thermal annealing was then performed in a high-vacuum chamber at $280 \degree C$ for 1 h, under an external magnetic field of 0.4 T in the direction normal to the multilayers. The $Co_{40}Fe_{40}B_{20}$ layer thickness and the annealing temperature were chosen such that spin reorientation transition occurs near room temperature.

Temperature-dependent magnetotransport and noise measurements were performed using a Quantum Design® Physical Property Measurement System (PPMS). A two-channel cross correlation method was used in the noise measurement.[21] The details of the noise measurement setup can be found in our previous work.[22] DC of 1 mA was applied to current leads of the Hall bar during the measurement. Sensitivity of the AHE sensor was measured by applying a modulating field ($\delta H = 0.3$ Oe) at 5 Hz and measuring the Hall voltage response. Previous work on tunneling magnetoresistance (TMR) sensors has found that the AC sensitivity measurement gives a more accurate estimation of the actual sensitivity, particularly when the TMR-field transfer curve is hysteretic.[23–25] Both noise and sensitivity were measured as sweeping the perpendicular field H_z from 300 Oe to −300 Oe, while the anomalous Hall resistance was measured as sweeping the field along both directions. As PPMS uses a superconducting magnet to apply the magnetic field, there could be relatively large errors at low fields. To remove the trapped magnetic flux, before our measurement, we have set the superconducting magnet from a large field to zero in

oscillating mode. In addition, we have reset the current in the superconducting magnet at each field step. To test the accuracy in the magnetic field, separate magnetotransport measurements were also performed at room temperature with a pair of calibrated electromagnets.

Figure 1(b) shows the anomalous Hall resistance R_H as a function of the perpendicular magnetic field H_Z at various temperatures. As temperature increases, the saturation field increases, implying that the perpendicular anisotropy becomes weaker. The temperature dependence of the anisotropy is consistent with previous experimental and theoretical work.[19,20] At 250 K, a small saturation field of 15 Oe is observed; yet, a very small coercivity of 0.5 Oe is also present. The small coercivity indicates that the $Co_{40}Fe_{40}B_{20}$ layer has an effective positive perpendicular anisotropy, possibly giving rise to the multidomain structure. Such small hysteresis might have been overlooked in previous work,[4,8,9,17] where the hysteresis-free behavior has been claimed. As shown in the later discussion, this small coercivity has significant effects on both low-frequency noise and sensitivity of the AHE sensor. When increasing the temperature from 250 K to a higher temperature, a transformation occurs around zero magnetic field. In this region, as presented in the inset in Fig. 1(b), a minor hysteresis loop emerges with a small perpendicular magnetic field offset. This minor hysteresis loop has also been observed in room-temperature measurements with a pair of calibrated electromagnets, which excludes potential artifacts from the superconducting magnet of PPMS. The presence of a minor hysteresis loop has also been reported in $Co_{52.5}Fe_{22.5}B_{25.0}$ with strain-controlled perpendicular magnetic anisotropy.[26] Both the minor hysteresis loop and the small field offset can be explained by the inhomogeneity of the magnetic anisotropy, which may originate from interface roughness or the boundary effect. Due to the inhomogeneity, some regions of the $Co_{40}Fe_{40}B_{20}$ layer have stronger perpendicular anisotropies than other regions. Also, exchange couplings between regions with different magnetic anisotropies give rise to the perpendicular magnetic field offset. The Hall resistance in saturation regions decreases with the increasing temperature, due to the reduction of the saturation magnetization and/or anomalous Hall coefficient. From the temperature-dependent magnetotransport measurement, we confirm that the average effective perpendicular anisotropy of the AHE sensor changes from positive at 250 K to negative at 350 K, with spin-reorientation transition occurring around room temperature (300 K).

With the knowledge from magnetotransport results, we then performed the noise measurement in a narrower range of magnetic fields from −35 Oe to 35 Oe. Combining the voltage noise S_V (in units of V^2/Hz) and sensitivity s (in units of Ω/T), we can determine the

FIG. 1. (a) Schematics of the Hall bar and multilayer structure. The Hall bar leads are electrically connected to Cr/Au electrodes. The total area of the Hall bar is $500 \times 500 \ \mu m^2$, while the effective sensing area is $20 \times 20 \ \mu m^2$. (b) Hall resistance vs external magnetic field at various temperatures. The four representative points shown in Fig. 2 are circled in AHE loops. The inset shows the AHE curve near zero field.

FIG. 2. Representative (a) noise and (b) field detectability spectra at various external fields and temperatures. In (a), the background noise of the noise measurement system is indicated by a dashed line.

magnetic field detectability $S_T = \frac{S_V}{(Is)^2}$, where I is the bias current. In the following text, we present the results of $S_T^{0.5}$ (in units of $T/\sqrt{Hz}$) to compare with others' work. We have chosen four representative noise and detectability spectra, as presented in Figs. 2(a) and 2(b), respectively, which correspond to (1) in the saturation region, (2) in the intermediate field region, and (3) and (4) at different temperatures and at zero magnetic field, to give a clear presentation. At zero field, the largest $1/f$ noise is observed, while sensitivity is also the highest (5860 Ω/T at 260 K and 8724 Ω/T at 310 K). As a consequence, the low-frequency detectability is bad; yet, the high-frequency detectability is the best. In the saturation region, $1/f$ noise is reduced by five orders of magnitude. This demonstrates the magnetic origin of $1/f$ noise observed at lower magnetic fields. Nevertheless, due to the low sensitivity (76 Ω/T) in the saturation region, the field detectability is the worst. Under an intermediate external magnetic field, modest $1/f$ noise and sensitivity (2458 Ω/T) have been observed, which actually leads to the best low-frequency detectability. From these representative spectra, it can be seen that simply reducing noise or increasing sensitivity does not necessarily gives the best performance of the AHE sensor.

To better show noise behavior at various temperatures and external fields, we plot the noise map at a low frequency (1 Hz) and a high frequency (10 kHz) in Figs. 3(a) and 3(b), respectively. Figure 3(a) shows that the $1/f$ noise oscillates, with a broad and a narrow peak at 250 K and 310 K, respectively, around zero magnetic field. Comparatively, the high-frequency noise shows a much weaker temperature and magnetic field dependence. It should be noted that both saturation magnetization and the anomalous Hall coefficient should change gradually and smoothly in such a temperature range, which is much lower than the Curie temperature. Therefore, the change in either saturation magnetization or the anomalous Hall coefficient cannot account for the drastic and non-monotonic change of the $1/f$ noise. The sensitivity map, as presented in Fig. 3(c), shows similar behavior to $1/f$ noise below 320 K. Surprisingly, the AC sensitivity measurement gives the maximum sensitivity (8700 Ω/T) at 310 K, near spin
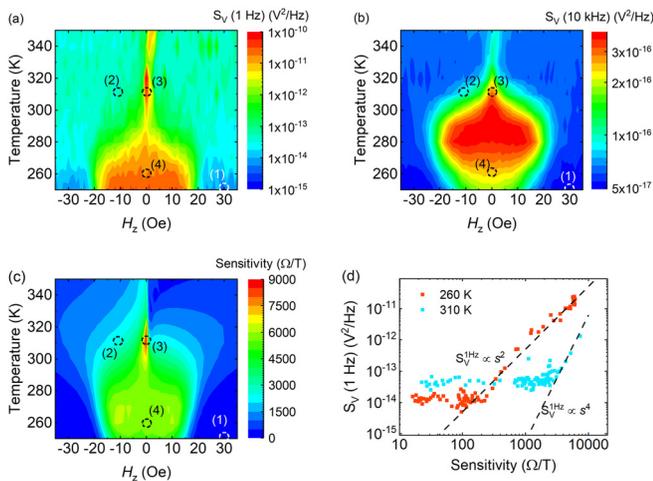
reorientation transition, while the sensitivity at zero field at 250 K is only 5400 Ω/T, almost half of the slope of the anomalous Hall loop (8040 Ω/T). The reduction in sensitivity at low temperatures is attributed to the hysteretic behavior of anomalous Hall loops, similar to that observed in magnetic tunnel junction (MTJ) sensors.[23–25] Since small coercivity may be easily overlooked in magnetotransport measurements, the AC sensitivity measurement is essential for determining the actual sensitivity of AHE sensors. At even a higher temperature, sensitivity becomes asymmetric with respect to the external field. It is noteworthy that no such significant asymmetry has been observed either in anomalous Hall loops or in the noise map. We have repeated the measurement on other samples, and similar behavior has also been observed. The asymmetry of the field dependence of sensitivity may originate from chirality induced by the interfacial Dzyaloshinskii–Moriya interaction (DMI); yet, the physical mechanism remains unclear. Also, the mismatch between noise and sensitivity implies that noise and sensitivity may be contributed by different regions of the $Co_{40}Fe_{40}B_{20}$ thin film, due to the inhomogeneity of magnetic anisotropy.

We plot the intrinsic noise (S_V) at 1 Hz against sensitivity for 260 K and 310 K, respectively, as shown in Fig. 3(d), to understand the two peaks of $1/f$ noise and their interplay with sensitivity. When sensitivity is low, $1/f$ noise remains constant for both temperatures. Such low sensitivity is achieved only under a large magnetic field (>100 Oe) and, thus, not shown in the contour plots for clarity. However, as sensitivity increases, $1/f$ noise follows different scaling relations with sensitivity ($S_V \propto s^2$ for 260 K and $S_V \propto s^4$ for 310 K). Although there has been no work on the scaling relation of $1/f$ noise with sensitivity in AHE sensors, we can compare our results with those from magnetoresistive (MR) sensors, where $1/f$ noise also originates from thermal magnetic fluctuations. In MR sensors, a linear scaling relation has been reported by many research groups.[27–38] The linear scaling relation can be understood from fluctuation-dissipation theorem.[27–29] On the other hand, a quadratic scaling relation has also been observed,[23,24,39–42] and there has been no good explanation on it. In a superparamagnetic MTJ, a quadratic scaling was observed in the ferromagnetic state, while a linear scaling was observed in the superparamagnetic state.[22] It was hypothesized that thermal equilibrium is reached only in the superparamagnetic state, resulting in the linear scaling, and the quadratic scaling relation results from non-equilibrium of the ferromagnetic state. For our AHE sensor, the quadratic scaling relation at 260 K may be explained by similar argument that the broad peak of $1/f$ noise at 250 K originates from magnetic hysteresis and domain wall hopping.[39] Nevertheless, there has been no report on the quartic scaling relation and its physical origin remains

FIG. 3. Map of voltage noise of the AHE sensor (a) at 1 Hz and (b) and 10 kHz. (c) Map of sensitivity of the AHE sensor, measured at 5 Hz. The four representative points shown in Fig. 2 are circled in these maps. (d) Voltage noise at 1 Hz vs sensitivity on the log–log scale. Data at 260 K and 310 K are shown in the plot.
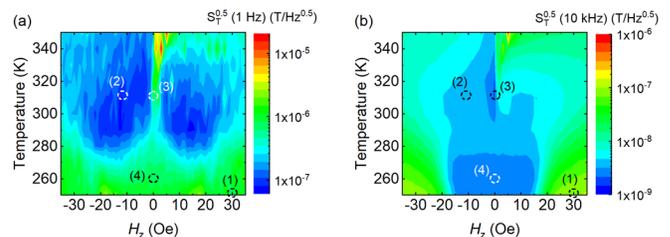
FIG. 4. Map of field detectability (a) at 1 Hz and (b) at 10 kHz. The four representative points shown in Fig. 2 are circled in these maps.

TABLE I. Multilayer structure of the AHE sensors, annealing condition, and sheet resistance R_{SH} of the AHE sensors. Three operating conditions (temperature T and bias field H_B) are tabulated, which give optimal performance either at low frequency or at high frequency.

Structure	Annealing condition	R_{SH} (kΩ/sq)	T (K)	H_B (Oe)	Sensitivity (Ω/T)	$S_T^{0.5}$ at 1 Hz (nT/$\sqrt{\text{Hz}}$)	$S_T^{0.5}$ at 10 kHz (nT/$\sqrt{\text{Hz}}$)
Ta(1.6)/Co$_{40}$Fe$_{40}$B$_{20}$(0.9)/ MgO(1.6)	280 °C at 0.4 T	3	310	−12	2458	76	4
			310	0	8724	668	2
			260	0	5859	684	3

unclear. As large magnetic fluctuation is expected near spin reorientation transition, the quartic scaling relation may be related to this phase transition. Much theoretical work is required to fully understand this emerging scaling relation.

From the definition of the field detectability ($S_T = \frac{S_V}{(Is)^2} \propto \frac{S_V}{s^2}$), a quadratic scaling relation implies that field detectability remains unchanged with respect to increasing sensitivity (S_T = const.), while a quartic scaling relation indicates that field detectability actually gets worse for a higher sensitivity ($S_T \propto \frac{S_V}{s^2} \propto s^2$). This could explain why low-frequency detectability is bad at zero field (high sensitivity), but best in the intermediate field region (moderate sensitivity), as presented in Fig. 2(b). Nevertheless, the quartic scaling relation also implies that the best detectability is only achieved at the "corner" sensitivity, where sensitivity is large but not so large as to boost the $1/f$ noise. In other words, the dynamic range of the AHE sensor with optimal detectability would be quite narrow. It should be noted that these results are not limited to noise and detectability at 1 Hz, but applicable to a wide frequency range where $1/f$ noise dominates.

Finally, we plot the maps of field detectability at 1 Hz and 10 kHz, which are shown in Figs. 4(a) and 4(b), respectively. As expected from the quadratic scaling relation ($S_V \propto s^2 \Rightarrow S_T \propto \frac{S_V}{s^2}$ = const.), low-frequency detectability is almost constant in a wide range of temperatures from 250 K to 270 K, as well as in a wide range of external fields from −30 Oe to 30 Oe. In the temperature range of 270 K to 320 K, field detectability reaches the minimum under a finite external field, due to the quartic scaling relation between $1/f$ noise and sensitivity. The best field detectability reaches 76 nT/$\sqrt{\text{Hz}}$ at 1 Hz, comparable to TMR sensors.[22,40] It should be emphasized that the sensing area of these TMR sensors is as large as 1 mm^2, while our AHE sensor has a much smaller sensing area of 400 μm^2. If the same sensing area is used, our AHE sensor actually outperforms these TMR sensors in the low-frequency region. At high frequency, the field detectability map closely resembles the sensitivity map, as the high-frequency noise changes only by a small amount. The best high-frequency detectability reaches 2 nT/$\sqrt{\text{Hz}}$ at 10 kHz. The operating conditions for the best detectability and characterization results are summarized in Table I. Compared to our previous work on FePt alloys with an in-plane anisotropy,[5] the field detectability is improved by two and one order of magnitude, respectively, at low and high frequencies, while the anomalous Hall angle is actually smaller. As can be seen from Fig. 4(a), the AHE sensor only achieves such superior low-frequency detectability in a narrow range of 10 Oe. Nevertheless, this dynamic range may be sufficient for applications where ultra-small magnetic signals are to be detected, and external magnetic field biasing is applicable.

In summary, we have fabricated an AHE sensor based on the Ta/Co$_{40}$Fe$_{40}$B$_{20}$/MgO multilayer structure and performed magnetotransport

and noise measurements in the 250 K–350 K range. We have found that both $1/f$ noise and sensitivity, as well as scaling relations between $1/f$ noise and sensitivity, change dramatically with varying temperature. When the effective perpendicular anisotropy is positive at low temperatures, $1/f$ noise scales quadratically with sensitivity. The quadratic scaling is attributed to the presence of magnetic hysteresis and domain wall hopping. Magnetic hysteresis also induces a large suppression of sensitivity, which demonstrates the necessity of the AC sensitivity measurement. Near spin reorientation transition around room temperature, the enhanced magnetic fluctuation gives rise to an emerging quartic scaling between $1/f$ noise and sensitivity. With a small sensing area of 20 × 20 μm^2, the best field detectability (76 nT/$\sqrt{\text{Hz}}$ at 1 Hz and 2 nT/$\sqrt{\text{Hz}}$ at 10 kHz) is comparable to or even outperforms TMR or giant magnetoresistance (GMR) sensors. As AHE sensors detect the perpendicular component of the magnetic field, it can also serve as a complement for TMR or GMR sensors, where the in-plane component of the magnetic field is sensed. Our work has shown that the AHE sensor with compensated magnetic anisotropies can have superior detectability. Moreover, since the Ta/Co$_{40}$Fe$_{40}$B$_{20}$/MgO structure is widely used in magnetic tunnel junctions (MTJs),[22,25,40,43] it would be very interesting to fabricate TMR sensors whose magnetic free layers have compensated magnetic anisotropies. Since the TMR effect is much larger than the AHE, even higher sensitivities can be expected.

AUTHORS' CONTRIBUTIONS

Y.Z. and K.W. contributed equally to this work.

DATA AVAILABILITY

The data that support the findings of this study are available from the corresponding author upon reasonable request.

REFERENCES

[1] E. Liu, Y. Sun, N. Kumar, L. Muchler, A. Sun, L. Jiao, S. Y. Yang, D. Liu, A. Liang, Q. Xu et al., Nat. Phys. **14**(11), 1125 (2018).
[2] C. Shekhar, N. Kumar, V. Grinenko, S. Singh, R. Sarkar, H. Luetkens, S. C. Wu, Y. Zhang, A. C. Komarek, E. Kampert et al., Proc. Natl. Acad. Sci. U. S. A. **115**(37), 9140 (2018).
[3] T. Suzuki, R. Chisnell, A. Devarakonda, Y. T. Liu, W. Feng, D. Xiao, J. W. Lynn, and J. G. Checkelsky, Nat. Phys. **12**(12), 1119 (2016).
[4] Y. M. Lu, J. W. Cai, H. Y. Pan, and L. Sun, Appl. Phys. Lett. **100**(2), 022404 (2012).
[5] Y. Zhang, Q. Hao, and G. Xiao, Sensors **19**(16), 3537 (2019).

[6]Y. Ni, Z. Zhang, I. C. Nlebedim, and D. C. Jiles, IEEE Trans. Magn. **52**(7), 1 (2016).

[7]N. Nagaosa, J. Sinova, S. Onoda, A. H. MacDonald, and N. P. Ong, Rev. Mod. Phys. **82**(2), 1539 (2010).

[8]T. Zhu, P. Chen, Q. H. Zhang, R. C. Yu, and B. G. Liu, Appl. Phys. Lett. **104**(20), 202404 (2014).

[9]Y. Zhu and J. W. Cai, Appl. Phys. Lett. **90**(1), 012104 (2007).

[10]I. Fergen, K. Seemann, A. von der Weth, and A. Schuppen, J. Magn. Magn. Mater. **242-245**, 146 (2002).

[11]Y. Satake, K. Fujiwara, J. Shiogai, T. Seki, and A. Tsukazaki, Sci. Rep. **9**(1), 3282 (2019).

[12]G. X. Miao and G. Xiao, Appl. Phys. Lett. **85**(1), 73 (2004).

[13]Q. Hao, W. Z. Chen, S. T. Wang, and G. Xiao, J. Appl. Phys. **122**(3), 033901 (2017).

[14]H. X. Yang, M. Chshiev, B. Dieny, J. H. Lee, A. Manchon, and K. H. Shin, Phys. Rev. B **84**(5), 054401 (2011).

[15]B. Dieny and M. Chshiev, Rev. Mod. Phys. **89**(2), 025008 (2017).

[16]K. Wang, L. Qian, W. Chen, S.-C. Ying, G. Xiao, and X. Wu, Phys. Rev. B **99**(18), 184410 (2019).

[17]W. L. Peng, J. Y. Zhang, L. S. Luo, G. N. Feng, and G. H. Yu, J. Appl. Phys. **125**(9), 093906 (2019).

[18]J. Shiogai, Z. Jin, Y. Satake, K. Fujiwara, and A. Tsukazaki, Appl. Phys. Express **12**(12), 123001 (2019).

[19]J. G. Alzate, P. K. Amiri, G. Q. Yu, P. Upadhyaya, J. A. Katine, J. Langer, B. Ocker, I. N. Krivorotov, and K. L. Wang, Appl. Phys. Lett. **104**(11), 112410 (2014).

[20]H. Sato, P. Chureemart, F. Matsukura, R. W. Chantrell, H. Ohno, and R. F. L. Evens, Phys. Rev. B **98**(21), 214428 (2018).

[21]M. Sampietro, L. Fasoli, and G. Ferrari, Rev. Sci. Instrum. **70**(5), 2520 (1999).

[22]Y. Zhang, G. Y. He, X. X. Zhang, and G. Xiao, Appl. Phys. Lett. **115**(2), 022402 (2019).

[23]D. Mazumdar, X. Y. Liu, B. D. Schrag, M. Carter, W. F. Shen, and G. Xiao, Appl. Phys. Lett. **91**(3), 033507 (2007).

[24]D. Mazumdar, W. F. Shen, X. Y. Liu, B. D. Schrag, M. Carter, and G. Xiao, J. Appl. Phys. **103**(11), 113911 (2008).

[25]G. Y. He, Y. Zhang, L. J. Qian, G. Xiao, Q. Zhang, J. C. Santamarina, T. W. Patzek, and X. X. Zhang, Appl. Phys. Lett. **113**(24), 242401 (2018).

[26]Z. P. Shi, X. M. Liu, and S. D. Li, Chin. Phys. B **26**(9), 097601 (2017).

[27]S. Ingvarsson, G. Xiao, S. S. Parkin, W. J. Gallagher, G. Grinstein, and R. H. Koch, Phys. Rev. Lett. **85**(15), 3289 (2000).

[28]L. Jiang, E. R. Nowak, P. E. Scott, J. Johnson, J. M. Slaughter, J. J. Sun, and R. W. Dave, Phys. Rev. B **69**(5), 054407 (2004).

[29]H. T. Hardner, M. B. Weissman, M. B. Salamon, and S. S. Parkin, Phys. Rev. B **48**(21), 16156 (1993).

[30]J. F. Feng, Z. Diao, G. Feng, E. R. Nowak, and J. M. D. Coey, Appl. Phys. Lett. **96**(5), 052504 (2010).

[31]Z. Q. Lei, T. Zeng, G. Feng, P. J. Chen, P. T. Lai, and P. W. Pong, IEEE Trans. Magn. **48**(11), 3712 (2012).

[32]L. Jiang, J. F. Skovholt, E. R. Nowak, and J. M. Slaughter, paper presented at the Fluctuations and Noise in Materials, 2004.

[33]L. Jiang, A. Gokce, F. C. S. da Silva, and E. R. Nowak, paper presented at the Noise and Information in Nanoelectronics, Sensors, and Standards III, 2005.

[34]A. Ozbay, A. Gokce, T. Flanagan, R. A. Stearrett, E. R. Nowak, and C. Nordman, Appl. Phys. Lett. **94**(20), 202506 (2009).

[35]Z. Diao, E. R. Nowak, K. M. Haughey, and J. M. D. Coey, Phys. Rev. B **84**(9), 094412 (2011).

[36]J. Y. Chen, N. Carroll, J. F. Feng, and J. M. D. Coey, Appl. Phys. Lett. **101**(26), 262402 (2012).

[37]Y. Guo, J. Y. Wang, R. M. White, and S. X. Wang, Appl. Phys. Lett. **106**(21), 212402 (2015).

[38]G. Hui-Qiang, T. Wei-Yue, L. Liang, W. Jian, L. Da-Lai, F. Jia-Feng, and H. Xiu-Feng, Chin. Phys. B **24**(7), 078504 (2015).

[39]C. Ren, X. Y. Liu, B. D. Schrag, and G. Xiao, Phys. Rev. B **69**(10), 104405 (2004).

[40]W. Z. Zhang, Q. Hao, and G. Xiao, Phys. Rev. B **84**(9), 094446 (2011).

[41]B. Zhong, Y. Chen, S. Garzon, T. M. Crawford, and R. A. Webb, J. Appl. Phys. **109**(7), 07C725 (2011).

[42]T. Arakawa, T. Tanaka, K. Chida, S. Matsuo, Y. Nishihara, D. Chiba, K. Kobayashi, T. Ono, A. Fukushima, and S. Yuasa, Phys. Rev. B **86**(22), 224423 (2012).

[43]Y. Zhang and G. Xiao, Phys. Rev. B **100**(22), 224402 (2019).